Proceedings of the 16th International Conference on Soil Mechanics and Geotechnical Engineering

doi:10.3233/978-1-61499-656-9-1685

Deformation mechanisms during uplift of buried pipes in sand

Mécanismes de déformation lors du soulèvement d'une conduite enterrée dans le sable

C.Y. Cheuk, D.J. White and M.D. Bolton
Department of Engineering, University of Cambridge, United Kingdom

ABSTRACT

To investigate the deformation mechanisms during uplift of a pipe buried in sand, a series of tests was conducted in a plane-strain calibration chamber. Image analysis was used to track the soil movement through a window. From an initial embedment of 3 diameters, a model pipe was extracted vertically whilst digital cameras captured the soil movement. Tests were conducted in uniform silica sands with grain sizes varying over one order of magnitude. During uplift, wide zones of distributed shear developed between the pipe shoulders and the ground surface. Beyond peak resistance, the deformation localised into thin shear bands, leading to strain softening behaviour. Particle size did not affect peak uplift resistance or mobilisation distance for the chosen grain size range and cover depth.

RÉSUMÉ

Afin d'étudier les mécanismes de déformation lors du soulèvement d'une conduite enterrée dans le sable, des essais en contrainte plane ont étés effectués. Un modèle de conduite enterré à une profondeur de trois diamètres dans un sable siliceux uniforme a été extrait verticalement en capturant les mouvements du sols avec des cameras digitales. Pendant le soulèvement, de larges zones de cisaillement apparaissent entre les piédroits de la conduite et la surface. Au-delà de la résistance de pointe, les déformations de cisaillement localisées dans de fines bandes donnent lieu à un comportement d'amollissement à l'effort. Pour la plage granulométrique étudiée et un rapport profondeur/diamètre constant, la taille des particules n'influence ni la résistance maximale au soulèvement ni la distance nécessaire à sa mobilisation.

1 INTRODUCTION

Subsea pipelines used for oil transportation are often buried to provide thermal insulation and reduce the risk of snagging on trawlgear. In order to ease the flow and prevent the solidification of wax fractions, it is necessary to raise the temperature and pressure of the contained oil. These operating conditions cause axial thermal expansion of the pipe. Such expansion is restricted by the side friction at the soil-pipe interface as well as the end connections which hold the pipe in position. Consequently, axial stresses are generated, that tend to cause buckling of the pipeline. The weakest mode of buckling is in the vertical plane, which can lead to exposure of the pipeline and failure in bending: this process is called upheaval buckling.

The backfilled soil cover prevents upheaval buckling by creating uplift resistance. This uplift resistance must be mobilised at a sufficiently small displacement to prevent buckle initiation. The cost of trenching and backfilling the entire length of a pipeline represents a significant portion of the total construction cost. It is therefore important to predict the minimum required burial depth required to generate sufficient uplift resistance at a small enough displacement for the pipeline to remain in stable equilibrium.

Current design methods for the prediction of uplift resistance in sand are highly empirical. Improved design efficiency would arise from a better understanding of the deformation mechanism above an uplifting pipe, and hence a better basis for calculating uplift resistance and mobilization distance. Since significant uncertainty exists in current design methods, site-specific small-scale model tests are widely used to evaluate uplift resistance. Comparison of model and field-scale experiments shows good agreement with respect to uplift resistance (White et al., 2001), but there are significant discrepancies in the mobilisation displacement, when expressed in the usual non-dimensional form as a fraction of the pipe diameter (Palmer et al., 2003).

This paper describes a series of model pipe uplift tests conducted to establish the deformation mechanisms during pipe uplift in sand. These tests were carried out in a transparent-sided plane-strain calibration chamber at approximately half-scale compared to field pipelines. An image analysis system based on particle image velocimetry (PIV) and close range photogrammetry was used to track the soil movement at many thousands of points within the model without recourse to intrusive target markers (White et al., 2003). The pipe was extracted vertically from a cover depth of 3 diameters at constant velocity whilst digital cameras captured the soil movement. Tests were conducted at two densities in two uniform silica sands with grain sizes differing by one order of magnitude.

2 EXPERIMENTAL DETAILS

2.1 *Test equipment*

A calibration chamber of inner dimensions 75.5 mm × 1000 mm × 835 mm, with a side window, provided plane strain test conditions and allowed deformation mechanisms to be observed. Side friction was reduced by sheets of glass on the inner walls of the chamber. A 100 mm diameter model pipe was made from a hollow brass tube and had a PTFE disc fitted on each end to reduce end friction. The pipe fitted sufficiently close between the faces of the chamber that ingress of sand between the pipe and the window was prevented. The end of the pipe was marked to allow the movement to be tracked by image analysis. An aluminium tie rod connected the pipe to a vertical actuator via a load cell. The tie rod was divided into 50 mm long segments which were screwed together sequentially during model preparation.

The vertical actuator comprised a stepper motor driving a machine screw mounted on the top of the calibration chamber. Three Kodak DC280 cameras were used to observe the first two tests, whilst two higher resolution Canon G3 cameras were used during the final two tests.

2.2 *Test materials*

Two gradings of uniform silica sand were used. Coarse Fraction A sand has a D_{50} size of 2.24 mm, and maximum and minimum void ratios of 0.83 and 0.55 respectively, which correspond to dry densities, ρ_d, of 1447 kg/m^3 and 1712 kg/m^3. Fine Fraction D sand has a D_{50} size of 0.28 mm, which is about 10 times smaller than that of Fraction A. The maximum and minimum void ratios of this finer sand are 1.01 and 0.68 respectively, which are slightly higher than those of Fraction A, possibly due to higher angularity. These limiting void ratios correspond to minimum and maximum densities of 1318 kg/m^3 and 1575 kg/m^3 respectively. Direct shear box tests showed a critical state friction angle, ϕ_{crit}, of 32° for both sands.

2.3 *Preparation and test procedure*

A set of black circular control markers printed onto transparent film were fixed between the front window and the inner glass plate. These control markers were used to calibrate the image-space PIV displacement measurements using close range photogrammetry, eliminating image distortion (White et al., 2003).

A pneumatic sand pouring system was used to ensure uniformity of the soil model. By adjusting the travel speed of the pourer, the drop height of the down pipe and the size of the outlet slot, sand layers of different density are obtained.

The model pipe was placed on top of the soil when the depth had reached the target position. Sand pouring continued to a cover depth, H, of 300 mm, creating a cover ratio, H/D, of 3.

2.4 *Image analysis*

A deformation measurement system based on Particle Image Velocimetry (PIV) and close range photogrammetry is described by White et al. (2003). Digital photography is used to capture images of planar soil deformation. Using PIV, the movement of a fine mesh of soil patches is measured to a high precision. Since PIV operates on the image texture, intrusive target markers need not be installed in the observed soil. The resulting displacement vectors are converted from image-space to object-space using photogrammetry. The locations of the control markers are used to calibrate the photogrammetric transformation. This transformation accounts for camera movement and image distortion (due to non-coplanarity of the object and image planes, refraction at the window and lens distortion).

2.5 *Test programme*

A series of four tests was conducted, using two grain sizes and two densities as shown in Table 1. For ease of comparison, an attempt was made to achieve the same relative density in one test of each grain size. However, a discrepancy of 6% was found after preparation of the second medium dense sample. The peak angles of friction, ϕ_{peak}, and dilation, ψ_{peak}, estimated by the procedure proposed by Bolton (1986) are also listed.

The uplift rate was 10 mm/hour in all tests. This rate was chosen to allow sufficient images to be obtained at the maximum frame rate of the cameras. During tests CD and CM, the maximum frame rate of the Kodak DC280 (1 per 90 seconds) corresponded to a 0.25 mm displacement increment per image. The Canon G3 has double this frame rate, leading to half the displacement increment.

Table 1. Summary of tests

Test	D_{50} (mm)	Dry density, ρ_d (kg/m^3)	Voids ratio, e	Relative density, I_D	ϕ_{peak}	ψ_{peak}
CD	2.24	1687	0.57	92%	52°	25°
CM	2.24	1532	0.73	36%	42.5°	13.1°
FD	0.28	1551	0.71	92%	52°	25°
FM	0.28	1386	0.91	30%	39.9°	9.9°

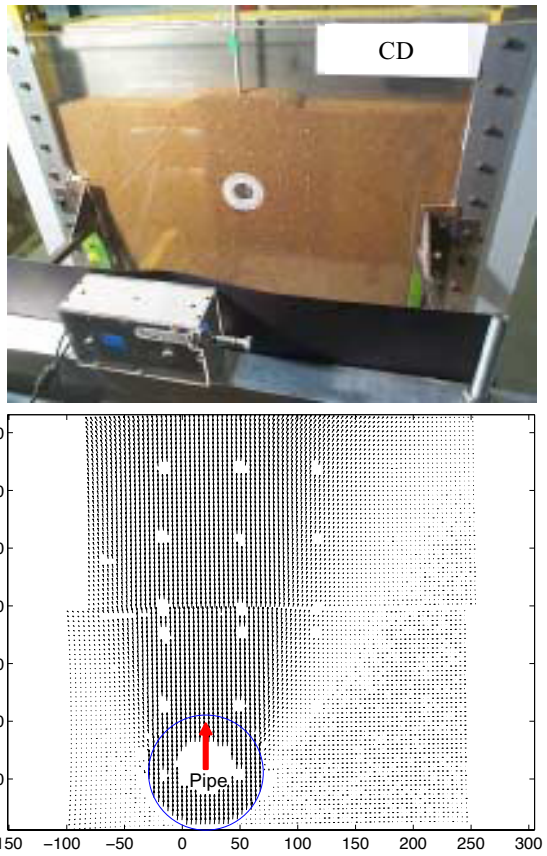

Figure 1. Experimental apparatus and example displacement vector field

3 RESULTS AND DISCUSSION

3.1 *Load-displacement response*

Figure 2 shows the variation of net uplift force (i.e. after subtracting the pipe weight) with pipe displacement. All four tests exhibit a stiff response in the first 0.5 mm, and reach a peak resistance at a pipe displacement of about 3 mm (+/- 5%) irrespective of density and grain size. The maximum uplift resistances in tests CD and FD are 127 N and 136 N respectively. The small (7%) difference reflects the similar peak angles of friction and dilation of these soil models (Table 1). The peak uplift resistance in test CM exceeds test FM by 28%. This discrepancy could be attributed to the higher peak angles of friction and dilation of the slightly denser coarse soil model.

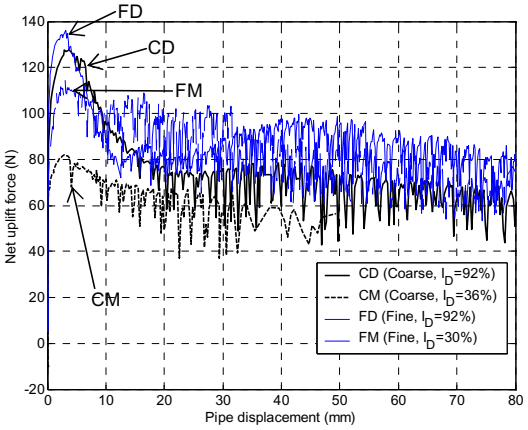

Figure 2. Measured uplift resistance

Post-peak softening is observed in all the tests. During the dense tests the uplift force drops by more than 40%. The force measurements become unsteady after a pipe displacement of ~10 mm. These oscillations coincide with small landslides of soil flow past the sides of the pipe into the void beneath. Each landslide exerts an upwards force on the invert of the pipe, reducing the force required for pullout. A similar phenomenon was observed by Trautmann et al. (1985) and Dickin (1994).

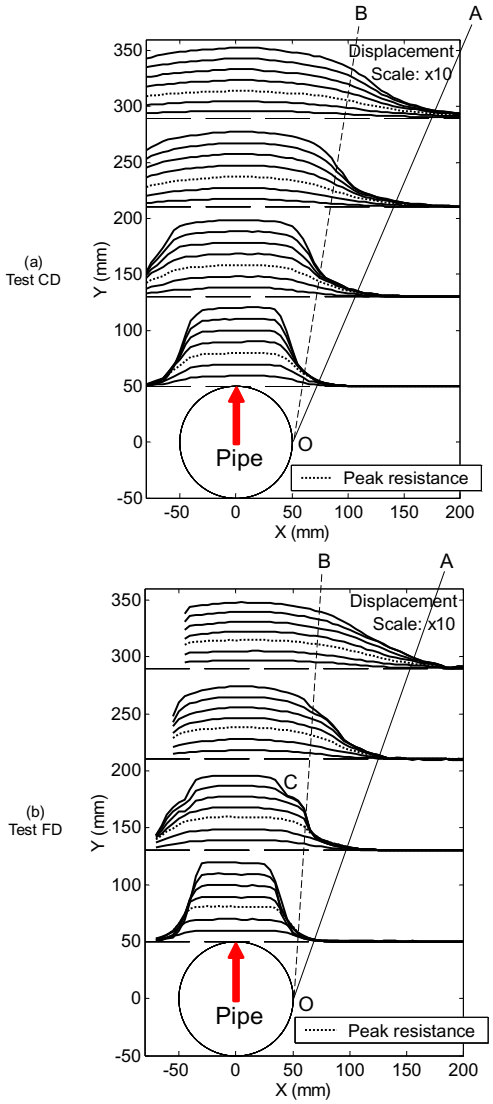

Figure 3. Vertical displacement profiles in coarse and fine sand
[Lines corresponds to 1 mm increments of pipe movement]

3.2 *Deformation measurements*

Due to space limitations, only the deformation measurements from the dense sand tests are discussed.

3.2.1 *Vertical soil displacement and shear banding*

Figure 3 shows the pattern of vertical displacements in tests CD and FD. Each curve represents the vertical movement at a given depth for ~1 mm increments of pipe movement up to 7 mm (0.07*D*). The gradient of these curves represents the horizontal variation in vertical displacement, which is approximately equal to the shear strain since the movement is primarily vertical.

The vertical displacement profiles for the two sands are similar in shape, especially at small pipe displacements. The soil immediately above the pipe moves as a block with minimal shear deformation, which is reflected by the straight displacement profiles above the pipe centreline. Prior to peak resistance, distributed shear deformation takes place within a line inclined at approximately 25° (OA) from the waist of the pipe. The similar deformation in the two sands at peak resistance substantiates the comparable mobilisation distances and peak resistances.

After peak resistance, the shear deformation localizes within a narrower shear zone, bounded by line OB. This shear zone is near-vertical, reflecting a drop in the dilation angle of the deforming soil. It is notable that in fine sand, after 6 mm of displacement, a second shear band forms (evident at point C in Fig 3b), whilst in coarse sand only a single shear band forms.

3.2.2 *Soil compression above the pipe centreline*

To examine the compression of the soil above the pipe, the total vertical displacement along the centreline is plotted in Figure 4. The reciprocal of the gradient of these curves (i.e. dv_{centre}/dy) represents the variation in total linear vertical strain above the pipe. The results for the two sands are very similar, especially at small pipe displacements up to peak resistance. A differential vertical movement between the surface and the pipe of ~0.7 mm is measured after a pipe movement of 3 mm, which corresponds to peak uplift resistance. This compression corresponds to a mean vertical strain of 0.23% in the soil column, and is caused by the increase in vertical stress as the pipe is pulled upwards.

The differential movement increases to ~1 mm beyond peak resistance. During this period, the uplift force, and hence the vertical stress, is reducing. However, the soil movement has a horizontal component away from the centerline, permitting further vertical compression to a total vertical strain of 0.33%.

To further examine the deformation in the soil column above the pipe, the incremental vertical displacement normalised by the corresponding incremental pipe displacement is plotted for three instances in Figure 5. The results show the vertical strain rate above the pipe reducing with pipe displacement. This reduction in vertical strain rate arises from the combined effects of a) the reduction in vertical stress (which causes vertical extension) and b) the horizontal component of deformation away from the centreline (which permits vertical compression).

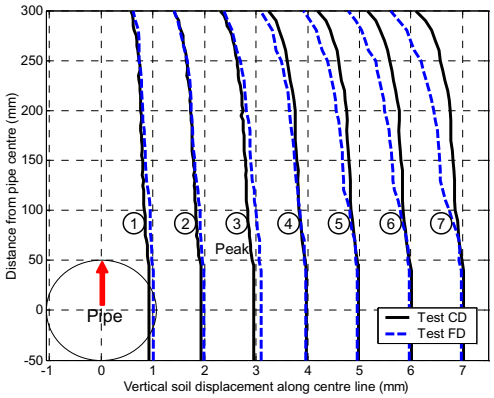

Figure 4. Vertical movement above the pipe centerline
[Numbers in circles represent the sequence of upward pipe movement]

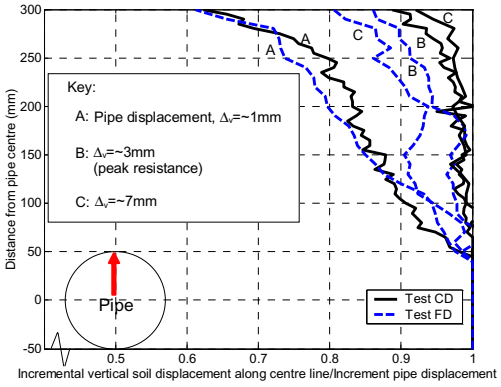

Figure 5. Incremental vertical movement above the pipe centerline

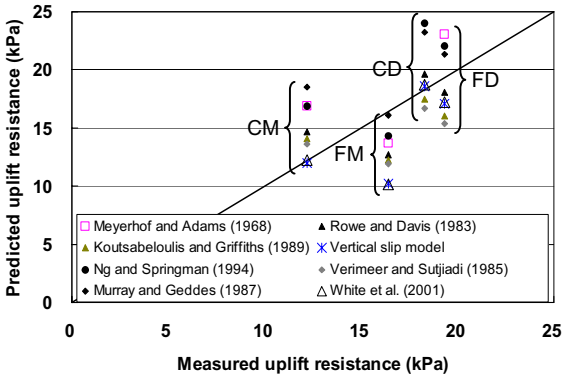

Figure 6. Comparison of predicted and measured uplift resistance

3.3 *Comparison of predicted and measured uplift resistance*

Figure 6 compares the measured uplift resistance in the four tests with predictions obtained from existing design equations proposed in the literature. These design equations are based on limit equilibrium solutions or finite element limit analyses and are reviewed in more detail by Cheuk (2005).

The smallest mean discrepancy between the measured and predicted results is found using the limit equilibrium method shown in Figure 7 and the uplift force (P) is given by.

$$P = \gamma HD + \gamma H^2 \tan\psi + \gamma H^2 (\tan\phi_{peak} - \tan\psi)\left[\frac{(1+K_0) - \cos 2\psi (1-K_0)}{2}\right] \quad (1)$$

This good agreement (albeit for a dataset of only 4 tests at only one embedment) can be linked to two assumptions in the design equation that match the observations obtained in the model tests. Firstly, the design equation includes shear zones inclined at the angle of dilation, ψ. A wide zone of displacement was observed in these experiments, extending outwards at the angle of dilation. Within the previous limit equilibrium solution, the shear zones are idealised as vertical planes.

Secondly, the method shown in Figure 7 assumes a shear stress distribution along the slip surface that exceeds the in situ value. The experimental results (Fig 6) show that the vertical stress at the pipe level is ~18 kPa at peak uplift in dense sand. This value exceeds the in situ stress, which is about 5 kPa. The solution shown in Figure 7 captures the increase in stress above the pipe by assuming that the normal stress on the slip planes remains a constant value corresponding to the in situ stress state. The vertical stress above the pipe is assumed to increase until the peak friction angle, ϕ_{peak}, is mobilised on the slip planes. The value of ϕ_{peak} is calculated from ϕ_{crit} and relative density following Bolton (1986).

It is interesting that no scale effect related to particle size is evident in these tests. The Palmer et al. (2003) model for pipe uplift hypothesises that a scale effect would be apparent if the shear zone above the pipe is characterised by localised shearing

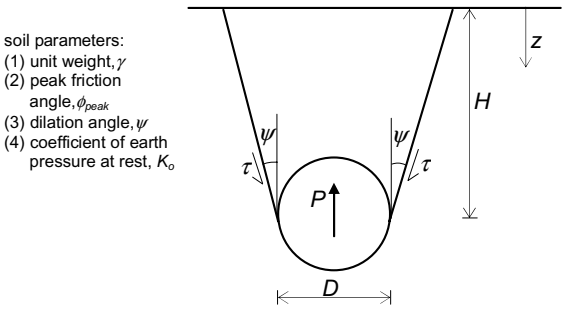

Figure 7. A model for the prediction of peak uplift resistance (White et al., 2001)

governed by a shear stress – displacement law and the soil column above the pipe is compressible. This model for progressive failure follows a similar logic to analyses for the progressive failure of long offshore piles in which a strain-softening t-z shaft resistance response causes flexible piles to exhibit a lower peak shaft capacity than rigid piles (Randolph 1983). Although compression is evident in these pipe uplift experiments, the difference between the surface and the pipe movements at peak uplift resistance is only 10%. Also, the observed deformation at peak uplift is not a concentrated shear band, likely to be governed by a stress-displacement law, but a distributed zone of shear deformation, which is more likely to be characterised by a stress-strain relationship.

4 CONCLUSIONS

The deformation mechanisms during uplift of a pipe buried in sand have been observed in a plane strain calibration chamber, and quantified using a new image analysis technique. In dense sand (I_D = ~92%), the failure deformation at peak resistance comprised a distributed shear zone bounded by planes inclined at the angle of dilation above the pipe. A drop in resistance beyond this peak was accompanied by the formation of narrow vertical shear bands.

Varying the mean particle size between 0.28 mm and 2.24 mm had a negligible effect on the peak uplift resistance and mobilisation distance. These measurements are in agreement with the observed soil displacement. The deformation pattern did not localise until after peak resistance. The distributed shear deformation at peak resistance is associated with stress-strain behaviour, which appears to be uninfluenced by particle size.

REFERENCES

Bolton, M.D. 1986. The strength and dilatancy of sands. *Géotechnique*, 36(1): 65-78.

Cheuk, C.Y. 2005. Soil-pipeline interaction at the seabed. *PhD thesis*, University of Cambridge.

Dickin, E.A. 1994. Uplift resistance of buried pipelines in sand. *Soils and Foundations*, 34(2): 41-48.

Kutsabeloulis, N. C. and Griffiths, D.V. 1989. Numerical modelling of the trap door problem. *Géotechnique*, 39(1): 77-89.

Meyerhof, G.G. and Adams, J.I. 1968. The ultimate uplift capacity of foundations. *Canadian Geotechnical Journal*, 5(4): 225-244.

Murray, E.J. and Geddes, J.D. 1987. Uplift of anchor plates in sand. *ASCE J. Geotechnical Engineering*, 113(3): 202-215.

Ng, C.W.W. and Springman, S.M. 1994. Uplift resistance of buried pipelines in granular materials. *Centrifuge 94*, Leung, Lee & Tan (eds), 753-758.

Palmer, A.C., White, D.J., Baumgard, A.J., Bolton, M.D., Barefoot, A.J., Finch, M., Powell, T., Faranski, A.S. and Baldry, J.A.S. 2003. Uplift resistance of buried submarine pipelines: comparison between centrifuge modelling and full-scale tests. *Géotechnique*, 53(10): 877-883.

Randolph M.F. 1983. Design considerations for offshore piles. *Proc. Conf. on Geotechnical Practice in Offshore Engineering,* Austin, Texas, 422-439

Rowe, R.K. and Davis, E.H. 1982. Behaviour of anchor plates in sand. *Géotechnique*, 32(1): 25-41

Trautmann, C.H., O'Rourke, T. D. and Kulhawy, F.H. 1985. Uplift force-displacement response of buried pipe. *Journal of Geotechnical Engineering*, 111(9): 1061-1076.

Vermeer, P.A. and Sutjiadi, W. 1985. The uplift resistance of shallow embedded anchors. *Proc. 11th Int. Conf. Soil Mechanics & Foundation Engineering*, (3): 1635-1638.

White, D.J., Barefoot, A.J. and Bolton, M.D. 2001. Centrifuge modelling of upheaval buckling in sand. *International Journal of Physical Modelling in Géotechnics*, 2(1): 19-28.

White, D.J., Take, W.A. and Bolton, M.D. 2003. Soil deformation measurement using particle image velocimetry (PIV) and photogrammetry. *Géotechnique*, 53(7): 619-631.